To appear in ApJ Letters
Preprint typeset using LaTeX style emulateapj v. 01/23/15

arXiv:1609.08771v2 [astro-ph.GA] 29 Sep 2016

SPATIALLY RESOLVED HCN ABSORPTION FEATURES IN THE CIRCUMNUCLEAR REGION OF NGC 1052

Satoko Sawada-Satoh[1,2], Duk-Gyoo Roh[3], Se-Jin Oh[3], Sang-Sung Lee[3,4], Do-Young Byun[3,4], Seiji Kameno[5,6], Jae-Hwan Yeom[3], Dong-Kyu Jung[3], Hyo-Ryoung Kim[3], Ju-Yeon Hwang[3,7]

To appear in ApJ Letters

ABSTRACT

We present the first VLBI detection of HCN molecular absorption in the nearby active galactic nucleus NGC 1052. Utilizing the 1 mas resolution achieved by the Korean VLBI Network, we have spatially resolved the HCN absorption against a double-sided nuclear jet structure. Two velocity features of HCN absorption are detected significantly at the radial velocity of 1656 and 1719 km s^{-1}, redshifted by 149 and 212 km s^{-1} with respect to the systemic velocity of the galaxy. The column density of the HCN molecule is estimated to be 10^{15}—10^{16} cm^{-2}, assuming an excitation temperature of 100—230 K. The absorption features show high optical depth localized on the receding jet side, where the free-free absorption occurred due to the circumnuclear torus. The size of the foreground absorbing molecular gas is estimated to be on approximately one-parsec scales, which agrees well with the approximate size of the circumnuclear torus. HCN absorbing gas is likely to be several clumps smaller than 0.1 pc inside the circumnuclear torus. The redshifted velocities of the HCN absorption features imply that HCN absorbing gas traces ongoing infall motion inside the circumnuclear torus onto the central engine.

Keywords: galaxies: active — galaxies: individual(NGC 1052) — galaxies: nuclei — radio lines: galaxies

1. INTRODUCTION

According to the most common active galactic nuclei (AGNs) model, i.e. the Unified Scheme of AGNs (Antonucci 1993), AGNs consist of a supermassive black hole (SMBH) or a central engine with a rotating dense gas disk or torus surrounding the SMBH. It is generally accepted that pronounced activity in an AGN is generated by accreting gas from its torus onto a SMBH. The distribution and kinematics of the circumnuclear gas are keys for understanding the fueling of the AGN.

High angular resolution studies of molecular gas in the center of the external galaxies (radius of ~ 1 kpc) have been obtained with millimeter interferometers. The size of the circumnuclear torus, however, is smaller than 10 pc (e.g. García-Burillo et al. 2016), and a milliarcsecond (mas) resolution is required to study its internal structure in nearby AGNs. While conventional millimeter interferometers, even ALMA, did not achieve such a high angular resolution, VLBI observations have revealed the parsec- or subparsec-scale morphology of nearby AGNs. Generally, thermal emission lines from molecular gas are not luminous enough to detect with the VLBI. VLBI maps, however, can display thermal absorption lines of the gas in silhouette against a bright background synchrotron radiation source with a mas resolution.

NGC 1052 is a nearby elliptical galaxy with a systemic velocity ($V_{\rm sys} = cz$) of 1507 km s^{-1} (Jensen et al. 2003), implying a distance of 20 Mpc assuming $H_0 = 75$ km s^{-1} Mpc^{-1} and $q_0 = 0.5$. Its nuclear activity is classified as occurring within a low-ionization nuclear emission-line region (LINER; e.g. Gabel et al. 2000). NGC 1052 has a nearly symmetric double-sided radio jet structure along the east–west direction from kiloparsec to parsec scales (e.g. Jones et al. 1984; Wrobel 1984; Kellermann et al. 1998). Past VLBI studies constrained the jet inclination angle to lie $\geq 57^\circ$ using the optically thin radio flux density of the twin jet (Kadler et al. 2004; Sawada-Satoh et al. 2008; Baczko et al. 2016). The parsec-scale jet structure shows a prominent gap between the eastern (approaching) and western (receding) jets at various centimeter wavelengths (e.g. Claussen et al. 1998; Vermeulen et al. 2003). VLBI images at 43 GHz, however, show an innermost component in the gap (Kadler et al. 2004; Sawada-Satoh et al. 2008). Kameno et al. (2001) proposed the existence of a parsec-scale circumnuclear torus consisting of cold dense plasma from the convex radio continuum spectra due to the free-free absorption (FFA) by the foreground plasma.

Besides the ionized gas, several atomic and molecular gases are also found toward the center of NGC 1052. An H_2O megamaser emission is detected at velocities by redshifted 50—350 km s^{-1} with respect to $V_{\rm sys}$ (Braatz et al. 1994, 2003; Kameno et al. 2005), and the H_2O maser gas lies on the inner components in the center of NGC 1052, where the plasma torus is obscured (Claussen et al. 1998; Sawada-Satoh et al. 2008). Neutral atomic hydrogen (H I), OH, HCO^+, HCN, CO tran-

[1] Mizusawa VLBI Observatory, National Astronomical Observatory of Japan, 2-12 Hoshigaoka-cho, Mizusawa-ku, Oshu, Iwate 023-0861, Japan; satoko.ss@nao.ac.jp
[2] Center for Astronomy, Ibaraki University, 2-1-1 Bunkyo, Mito, Ibaraki 310-8512, Japan; sss@mx.ibaraki.ac.jp
[3] Korea Astronomy and Space Science Institute, 776 Daedeokdaero, Yuseong, Daejeon 34055, Republic of Korea
[4] University of Science and Technology, 217 Gajeong-ro, Yuseong-gu, Daejeon 34113, Republic of Korea
[5] Joint ALMA Observatory, Alonso de Cordova 3107 Vitacura, Santiago 763 0355, Chile
[6] National Astronomical Observatory of Japan, 2-21-1 Osawa, Mitaka, Tokyo 181-8588, Japan
[7] SET system, 16-3 Gangnam-daero 8-gil, Seocho-gu, Seoul 06787, Korea

sitions are found toward the center of NGC 1052 as absorptions (van Gorkom et al. 1986; Omar et al. 2002; Liszt & Lucas 2004; Impellizzeri et al. 2008). The velocity range over which those absorption lines are observed spans from 1500 to 1800 km s^{-1}, redshifted with respect to $V_{\rm sys}$-like H_2O maser emission. These facts imply that ionized, neutral, and molecular gases coexist in the vicinity of the central engine.

To investigate the geometry and physical properties of the molecular gas in the circumnuclear region of NGC 1052, we have performed high-resolution observations toward HCN (1–0) absorption lines with the Korean VLBI Network (KVN). Here we show the first parsec-scale HCN (1–0) maps of the center of NGC 1052. One milliarcsecond corresponds to 0.095 pc in the galaxy.

2. OBSERVATIONS AND DATA REDUCTION

KVN observations of NGC 1052 were carried out in 2015 March, for a total on-source time of 7.5 hr. To achieve high sensitivity for the 3 mm HCN (1–0) absorption line observation, simultaneous dual-frequency data at the K (21700—21828 MHz) and W (88643—88871 MHz) bands were recorded using the KVN multi-frequency receiving system (Oh et al. 2011; Han et al. 2013). Two IFs of left hand circular polarization with a bandwidth of 128 MHz were used simultaneously. One was assigned to the W-band for HCN (1–0), and the other was tuned to the K-band, the reference frequency to track a rapid phase time variation at the W-band. The velocity coverage of one IF at the W-band was $\sim$ 400 km s^{-1}. NRAO 150 was also observed as a calibrator for phase and bandpass. The Mark5B system at a recording rate of 1024 Mbps was used for recording the data. The correlation was processed at the Korea–Japan Correlation Center (Yeom et al. 2009; Lee et al. 2015a). We corrected the visibility amplitude decrement due to the digital quantization loss and the characteristics of the KJCC, using the method of Lee et al. (2015b).

Calibration, data flagging, fringe fitting, and imaging were performed using the NRAO AIPS software. To track a rapid phase time variation at the W-band, we analyzed these data using the frequency phase transfer method, in which the phase solutions of the low-frequency band (K-band) are transferred to the high-frequency (W-band) by scaling by their frequency ratios (Middelberg et al. 2005; Rioja et al. 2011). Doppler correction was applied using the AIPS task CVEL. The continuum was subtracted with the AIPS task UVLSF in the (u, v) domain. We corrected the visibility phase using self-calibration with the averaged line-free channels, and applied the result of the self-calibration in the absorption line images. Therefore, the absorption and continuum images could be accurately overlaid with positional errors only limited by the thermal noise in the absorption images. Images were produced with natural weighting, and the resulting FWHM of the synthesized beam is 1.44×0.90 mas (0.137×0.085 pc in NGC 1052).

3. RESULTS

The HCN (1–0) absorption spectra toward NGC 1052 obtained with the KVN are shown in Figure 1. The velocity resolution is 10.5 km s^{-1}. Two velocity features of HCN absorption are detected, labeled as I and II. The deepest absorption feature, I, shows a peak at

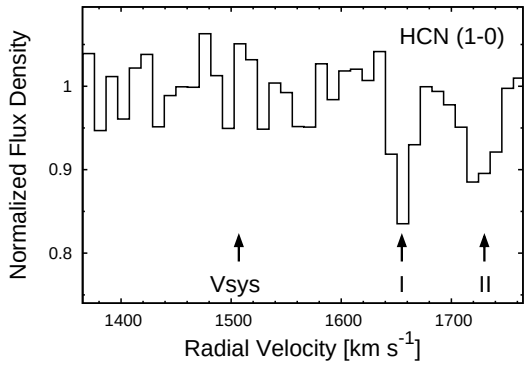

Figure 1. Spectral profile of the HCN (1–0) absorption line toward the center of NGC 1052 obtained with the KVN. Two velocity features of HCN absorption were detected at 1656 and 1719 km s^{-1}. We gave labels to the former (I) and the latter (II), respectively. The rms noise in the normalized flux density is 0.035.

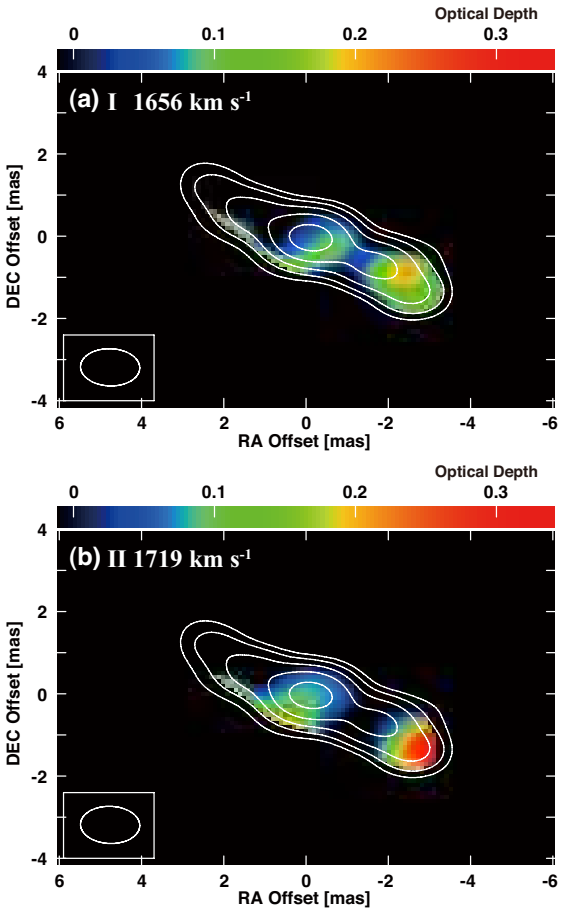

Figure 2. Color images of the HCN (1–0) optical depth of (a) feature I (1656 km s^{-1}) and (b) feature II (1719 km s^{-1}) in the circumnuclear region of NGC 1052, overlaid by a contour map of 89 GHz continuum emission. The contour starts at the 3σ level, increasing by a factor of 2, where σ = 3.9 mJy beam^{-1}. The absorption maps have achieved a 1 σ noise level of 4.6 mJy beam^{-1} in intensity, or $\sim$0.02 in optical depth. The velocity width of one channel map is 52.9 km s^{-1}.

1656 km s^{-1} channel and reaches -16% of the continuum level. The second-deepest absorption feature, II, reaches -10% of the continuum level at 1719 km s^{-1}. The two absorption features are also found in the absorp-

tion profile from the PdBI data (Liszt & Lucas 2004). The velocity widths and the peak velocities agree well with the profile measured using the PdBI, but the absorption depths in the spectral profile with the KVN are deeper than those of the PdBI (2—6%). Although Liszt & Lucas (2004) have shown several other absorption features with the depth of $\sim -3\%$ around 1500—1600 km s^{-1} from the PdBI data, our KVN data did not detect them significantly.

Figure 2 is a superposition of the line-free continuum image at 89 GHz and the opacity image for each HCN absorption feature. The continuum image reveals that a nearly symmetric double-sided radio jet structure along the east–west direction is elongated over ∼0.5 pc (contour map in Figure 2). The brightest continuum component is seen at the center of the elongated structure. The sum of all CLEAN components within 1.4 mas (the major axis of the synthesized beam) from the peak is 332 mJy, and it is $\sim 80\%$ of the value of the central continuum component at 86 GHz measured in 2004 October by the Global millimeter-VLBI Array (Baczko et al. 2016). The flux densities for the east and west jet are estimated to be 49 and 180 mJy, respectively. HCN opacity distribution against the double-sided radio jet structure shows that high opacities (> 0.2) are clearly found on the western receding jet side. Each opacity peak position of the absorption features I and II is offset by 0.24 and 0.27 pc, respectively, from the continuum peak position, where the central engine is supposed to exist.

4. DISCUSSIONS

4.1. *Absorbing Molecular Gas Properties*

The HCN opacity obtained from our observations was beyond 0.1 in the circumnuclear region of NGC 1052, and one order higher than that from the PdBI observations (Liszt & Lucas 2004). This indicates that the HCN covering factor is much smaller on the scale of a few hundreds parsecs. We estimated the mean opacity over the whole parsec-scale source structure $\langle\tau\rangle$, using

$$\langle\tau\rangle = \frac{\iint \tau(x,y) I(x,y)\, dx\, dy}{\iint I(x,y)\, dx\, dy} \qquad (1)$$

where $\tau(x,y)$ is the HCN opacity distribution shown in the color scale of Figure 2, and $I(x,y)$ is the 89 GHz continuum image. The estimated $\langle\tau\rangle$ is 0.027 and 0.028 for the absorption features I and II, respectively. They are on the same order of HCN opacity yielded from the normalized flux of 0.98 and 0.94 for the absorption features I and II observed with the PdBI (Liszt & Lucas 2004). Thus, the HCN covering factor is likely to be ~ 1 on parsec scales.

Under the assumption of the local thermodynamic equilibrium, and a covering factor of 1, the total molecular column density of the J=1–0 absorption line is derived as

$$N_{\rm tot} = \frac{3k}{8\pi^3\mu^2 B}\ \frac{(T_{\rm ex} + hB/3k)}{\left[1 - \exp\left(-h\nu/kT_{\rm ex}\right)\right]} \int \tau dv \qquad (2)$$

where k is the Boltzmann constant, h is the Planck constant, μ is the permanent dipole moment of the molecule, B is the rotational constant, $T_{\rm ex}$ is the excitation temperature, and $\int \tau dv$ is the velocity-integrated optical depth of the absorption feature.

Using the equation (2), $\mu = 2.98$ Debye, $B = 44315$ MHz for HCN, and assuming $\int \tau dv = \tau_{\rm max}\Delta v$, where $\tau_{\rm max}$ is the maximum of optical depth, we give the total column density of HCN for each absorption feature in Table 1. To determine the column density of molecular hydrogen (H_2), we assume a HCN-to-H_2 abundance ratio of 10^{-9}, from the HCN-to-H_2 abundance ratio estimates of $(0.2—4.1)\times10^{-9}$ of several HCN clumps in the Galactic Circumnuclear Disk (CND; Smith & Wardle 2014). Here we take $T_{\rm ex} = 100$ K and 230 K, as recent millimeter and submillimeter interferometric observations have detected the vibrationally excited HCN emission lines in the dust-enshrouded AGN of the luminous infrared galaxies (Sakamoto et al. 2010; Imanishi & Nakanishi 2013). The derived H_2 column density ($N_{\rm H_2}$) ranges 10^{24}—10^{25} cm^{-2}, using the values of $N_{\rm HCN}$ in Table 1. Hence, equivalent $N_{\rm H}$ would be of the same order as $N_{\rm H_2}$. It is one or two orders higher than the estimate of the $N_{\rm H} \sim 10^{23}$ cm^{-2} from modeling of X-ray spectra (Guainazzi & Antonelli 1999; Weaver et al. 1999; Guainazzi et al. 2000; Brenneman et al. 2009), and the electron column density of $\sim 10^{23}$ cm^{-2} estimated from the FFA opacity of the dense plasma (Sawada-Satoh et al. 2009).

4.2. *Circumnuclear torus model*

Kameno et al. (2005) and Sawada-Satoh et al. (2008) proposed that the circumnuclear torus consists of several phase layers. On the inner surface of the torus, a hot ($\sim$ 8000 K) plasma layer is formed by X-ray emission from the central engine and it causes FFA. A heated (above $\sim$ 400 K) molecular layer or X-ray dissociation region (XDR; Neufeld et al. 1994; Neufeld & Maloney 1995) lies next to the plasma layer, and the H_2O megamaser emission arises from here. As well as FFA opacity distribution, the HCN opacity shows high values on the western receding side of the jet. Thus, HCN absorbing gas could be associated with the torus, like the dense plasma. If $T_{\rm ex}$ of HCN is ~ 230 K, HCN molecules should lie in the cooler molecule layer next to XDR. The redshifted HCN absorption against the continuum emission is likely indicative of ongoing gas infall. The velocities of the HCN absorption features are close to the centroid velocity of the broad H_2O maser emission (~ 1700 km s^{-1}). Therefore, H_2O and HCN could trace the same infall motion inside the torus. The HCN absorption spectrum consists of at least two narrow absorption features, and HCN absorbing gas is more likely to be several small ($\leq$ 0.1 pc) clumps or layers with a different velocity, rather than a large homogeneous structure with a single velocity. We have seen the opacity contrast between the absorption features I and II, and the contrast also suggests the inhomogeneity inside the molecular torus. In Figure 3, we present a possible model for the geometry of the circumnuclear torus and the jet in NGC 1052. Since the jet axis is inclined from the sky plane, the near side of the torus should cover the receding jet side. The line of sight intersects at least two HCN gas clumps inside the torus.

As we have mentioned in Section 3, there is no signifi-

Table 1
Column density of HCN (1–0) absorption.

Label	$V_{\rm p}$ [km s^{-1}]	$V_{\rm p}-V_{\rm sys}$ [km s^{-1}]	Δv [km s^{-1}]	$\int \tau dv$ [km s^{-1}]	$N_{\rm HCN,100}$ [10^{14} cm^{-2}]	$N_{\rm HCN,230}$ [10^{14} cm^{-2}]
(1)	(2)	(3)	(4)	(5)	(6)	(7)
I	1656	149	31.7	9.3 ± 0.6	9.5 ± 0.6	50 ± 3
II	1719	212	52.9	19 ± 1	20 ± 1	101 ± 5

Note. — (1) Absorption feature ID, shown in Figure 1. (2) Peak velocity of the absorption feature. (3) Velocity with respect to $V_{\rm sys}$. (4) Line width. (5) Velocity-integrated optical depth. (6) HCN column density with $T_{\rm ex} = 100$ K. (7) HCN column density with $T_{\rm ex} = 230$ K.

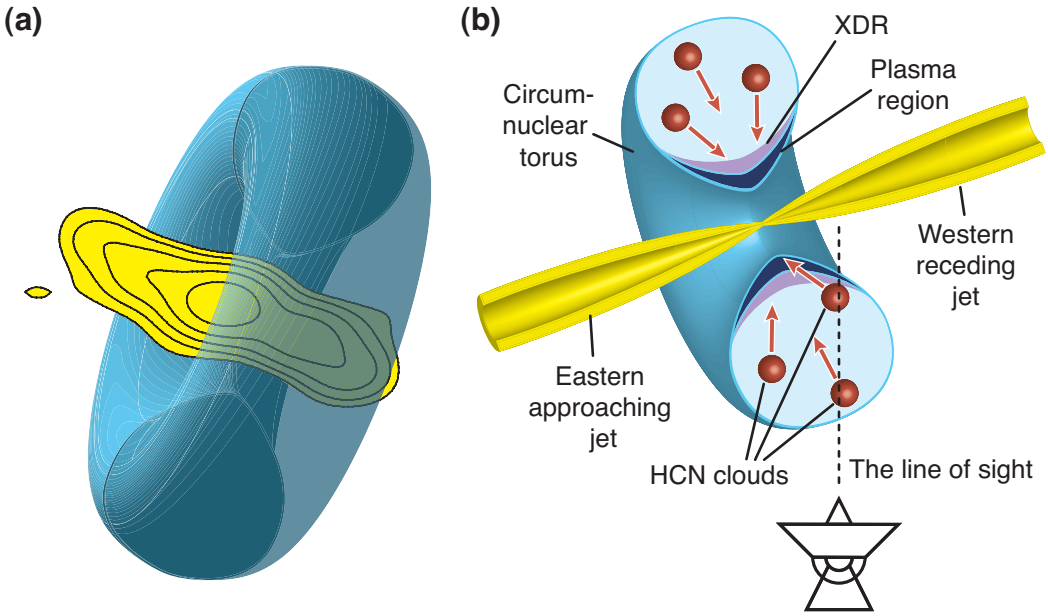

Figure 3. (a) Possible model of the oriented double-sided jet and the circumnuclear torus. The near side of the torus covers the receding jet side. (b) Schematic diagram for the intersection of the circumnuclear torus in NGC 1052. The torus has two-phase layers on the inner surface, the X-ray heated plasma region and the X-ray dissociation region (XDR). HCN absorbing gas is located in the cooler molecule region next to XDR. HCN absorbing gas could be clumpy, and the line of sight passes through several clumpy clouds with a different radial velocity.

cant detection of absorption features around 1500—1600 km s^{-1}, close to $V_{\rm sys}$. A possible explanation is that the missing absorption features could arise not from the compact molecular clumps in the circumnuclear region, but from the foreground diffuse interstellar medium in the host galaxy. If so, their covering factor would not vary on scales between a few parsecs and a few hundreds parsecs, and thus the depth of the absorption features would be $\sim -3\%$, the same as the PdBI results. It is comparable to the rms noise level of our spectral profile with the KVN, and no significant detection comes as a consequence. Furthermore, when their background continuum sources have a faint and extended structure, the background continuum emissions should be fully resolved-out. Therefore, the absorption features against the resolved-out background sources would be invisible in our KVN data.

We can estimate an approximate size of the foreground absorbing molecular gas using the relation $N_{\rm H_2} = f_v n_{\rm H_2} L$, where f_v is the volume filling factor, $n_{\rm H_2}$ is the molecular hydrogen volume density, and L is the size of the molecular gas. Here we simply assume $f_v = 0.01$. Adopting $N_{\rm H_2}$ of 10^{24}–10^{25} cm^{-2} from our results and $n_{\rm H_2}$=(0.1—2)$\times 10^6$ cm^{-3} in the Galactic CND (Smith & Wardle 2014), the resulting L is approximately on 1-pc scales. It is consistent with the approximate size of the circumnuclear torus of NGC 1052 (Kameno et al. 2001). On the other hand, the size of the innermost receding jet component can be estimated as 0.2—0.4 mas from the VLBA images at 43 GHz (Kadler et al. 2004; Sawada-Satoh et al. 2008), and it corresponds to 0.02—0.04 pc in linear scale.

Based on our measurements of the radial velocities and the distribution of HCN absorption features, the mass infall rate of the gas accretion toward the central engine can be estimated by $\dot{M} = f_v R_{\rm in}^2 \rho V_{\rm in} \Omega$, where f_v is the volume filling factor, $R_{\rm in}$ is an infall radius, ρ is the mass density of the infalling materials, $V_{\rm in}$ is the infall velocity, and Ω is the solid angle of the torus from the center. Here we assume $\rho = N_{\rm H} m_{\rm H}/R_{\rm in}$, where $N_{\rm H}$ is the column density of a hydrogen atom and $m_{\rm H}$ is the mass of a hydrogen atom. Giving $R_{\rm in} = 1$ pc, $N_{\rm H} = 10^{24}$—10^{25} cm^{-2}, and $V_{\rm in} = 200$ km s^{-1} as the approximate velocity of the HCN absorption feature with respect to $V_{\rm sys}$ ($V_{\rm p} - V_{\rm sys}$ in Table 1), the derived mass infall rate ranges $\dot{M} = (47$—$470)\ f_v(\Omega/4\pi) M_\odot$ yr^{-1}. If $(\Omega/4\pi)$ takes a few 0.1 and f_v is 0.01, it would be comparable to the calculation of the accretion rate of $10^{-1.39} M_\odot$ yr^{-1} from the hard X-ray luminosities by Wu & Cao (2006).

We note that the X-ray luminosity indicates an instantaneous accretion rate. However, our estimation of the accretion rate in the molecular torus gives a long-term ($R_{\rm in}/V_{\rm in} \sim 5000$ year) activity. The coincidence of the two accretion rate values suggests the continuity of AGN activity in NGC 1052.

5. SUMMARY

We have conducted 1 mas angular-resolution observations toward the HCN(1–0) absorption of the circumnuclar region in NGC 1052 with the KVN. Two HCN absorption features are identified and reach a depth of $\geq$ 10% from the continuum level at 1656 and 1719 km s^{-1}, redshifted with respect to $V_{\rm sys}$. We find an $N_{\rm HCN}$ of 10^{15}—10^{16} cm^{-2} in the center of NGC 1052, assuming an HCN covering factor of 1 and a $T_{\rm ex}$ of 100—230 K. The HCN opacity distribution against the double-sided radio continuum jet structure shows a localization of the HCN high opacity on the receding jet side. The size of the foreground absorbing molecular gas is estimated to be approximately on 1-pc scales. We argue that these results are most naturally explained by a circumnuclear torus that consist of several phase layers, perpendicular to the jet axis of NGC 1052. HCN absorbing gas distribution could be clumpy, and could be associated with the cooler molecular region inside the torus. The redshifted velocities of the HCN absorption features account for the infall motion onto the central engine, such as an H_2O megamaser emission.

We acknowledge the anonymous referee who provided constructive suggestions. We are grateful to all members of KVN for supporting our observations. S.S.S. would like to thank Yoshiharu Asaki and Taehyun Jung for their helpful discussions. S.S.L. was supported by the National Research Foundation of Korea(NRF) grant funded by the Korea government(MSIP) (No. NRF-2016R1C1B2006697). The KVN is a facility operated by the Korea Astronomy and Space Science Institute. The KVN operations are supported by the Korea Research Environment Open NETwork, which is managed and operated by Korea Institute of Science and Technology Information.

Facilities: KVN.

REFERENCES

Antonucci, R. 1993, ARA&A, 31, 473
Baczko, A.-K., Schulz, R., Kadler, M., et al. 2016, A&A, 593, A47
Braatz, J. A., Wilson, A. S., & Henkel, C. 1994, ApJL, 437, L99
Braatz, J. A., Wilson, A. S., Henkel, C., Gough, R., & Sinclair, M. 2003, ApJS, 146, 249
Brenneman, L. W., Weaver, K. A., Kadler, M., et al. 2009, ApJ, 698, 528
Claussen, M. J., Diamond, P. J., Braatz, J. A., Wilson, A. S., & Henkel, C. 1998, ApJL, 500, L129
Gabel, J. R., Bruhweiler, F. C., Crenshaw, D. M., Kraemer, S. B., & Miskey, C. L. 2000, ApJ, 532, 883
García-Burillo, S., Combes, F., Ramos Almeida, C., et al. 2016, ApJL, 823, L12
Guainazzi, M., & Antonelli, L. A. 1999, MNRAS, 304, L15
Guainazzi, M., Oosterbroek, T., Antonelli, L. A., & Matt, G. 2000, A&A, 364, L80
Han, S.-T., Lee, J.-W., Kang, J., et al. 2013, PASP, 125, 539
Imanishi, M., & Nakanishi, K. 2013, AJ, 146, 91
Impellizzeri, V., Roy, A. L., & Henkel, C. 2008, Proceedings of the 9th European VLBI Network Symposium on The role of VLBI in the Golden Age for Radio Astronomy, 33
Jensen, J. B., Tonry, J. L., Barris, B. J., et al. 2003, ApJ, 583, 712
Jones, D. L., Wrobel, J. M., & Shaffer, D. B. 1984, ApJ, 276, 480
Kadler, M., Ros, E., Lobanov, A. P., Falcke, H., & Zensus, J. A. 2004, A&A, 426, 481
Kameno, S., Sawada-Satoh, S., Inoue, M., Shen, Z.-Q., & Wajima, K. 2001, PASJ, 53, 169
Kameno, S., Nakai, N., Sawada-Satoh, S., Sato, N., & Haba, A. 2005, ApJ, 620, 145
Kellermann, K. I., Vermeulen, R. C., Zensus, J. A., & Cohen, M. H. 1998, AJ, 115, 1295
Lee, S.-S., Oh, C. S., Roh, D.-G., et al. 2015a, Journal of Korean Astronomical Society, 48, 125
Lee, S.-S., Byun, D.-Y., Oh, C. S., et al. 2015b, Journal of Korean Astronomical Society, 48, 229
Liszt, H., & Lucas, R. 2004, A&A, 428, 445
Middelberg, E., Roy, A. L., Walker, R. C., & Falcke, H. 2005, A&A, 433, 897
Neufeld, D.A., Maloney, P.R., & Conger, S. 1994, ApJ, 436, L127
Neufeld, D. A., & Maloney, P. R. 1995, ApJL, 447, L17
Oh, S.-J., Roh, D.-G., Wajima, K., et al. 2011, PASJ, 63, 1229
Omar, A., Anantharamaiah, K. R., Rupen, M., & Rigby, J. 2002, A&A, 381, L29
Rioja, M., Dodson, R., Malarecki, J., & Asaki, Y. 2011, AJ, 142, 157
Smith, I. L., & Wardle, M. 2014, MNRAS, 437, 3159
Sakamoto, K., Aalto, S., Evans, A. S., Wiedner, M. C., & Wilner, D. J. 2010, ApJL, 725, L228
Sawada-Satoh, S., Kameno, S., Nakamura, K., et al. 2008, ApJ, 680, 191-199
Sawada-Satoh, S., Kameno, S., Nakamura, K., Namikawa, D., & Shibata, K. M. 2009, Astronomische Nachrichten, 330, 249
van Gorkom, J. H., Knapp, G. R., Raimond, E., Faber, S. M., & Gallagher, J. S. 1986, AJ, 91, 791
Vermeulen, R. C., Ros, E., Kellermann, K. I., et al. 2003, A&A, 401, 113
Weaver, K. A., Wilson, A. S., Henkel, C., & Braatz, J. A. 1999, ApJ, 520, 130
Wrobel, J. M. 1984, ApJ, 284, 531
Wu, Q., & Cao, X. 2006, PASP, 118, 1098
Yeom, J. H., Oh, S. J., Roh, D. G., et al. 2009, Journal of Astronomy and Space Sciences, 26, 567